PCCP

COMMUNICATION

Simultaneous enhancement of magnetic and ferroelectric properties in Dy and Cr co-doped $BiFeO_3$ nanoparticles

Cite this: *Phys. Chem. Chem. Phys.*, 2016, **18**, 6399

Received 27th November 2015,
Accepted 28th January 2016

DOI: 10.1039/c5cp07327h

www.rsc.org/pccp

Weiwei Mao,[ab] Xingfu Wang,[ab] Liang Chu,[b] Yiyi Zhu,[a] Qi Wang,[a] Jian Zhang,[a] Jianping Yang,[b] Xing'ao Li*[a] and Wei Huang*[ac]

Multiferroic $BiFeO_3$ (BFO), $Bi_{0.95}Dy_{0.05}FeO_3$ and $Bi_{0.95}Dy_{0.05}Fe_{0.95}Cr_{0.05}O_3$ samples were successfully synthesized by a carbon microsphere-assisted sol–gel (CSG) method. X-ray diffraction analysis confirmed a lattice distortion from a rhombohedral structure to a tetragonal structure upon doping Dy and Cr in BFO. The morphology of BFO and doped BFO could be effectively controlled to form nanoparticles, due to the nucleation sites of the carbon microspheres. The co-doping of Dy and Cr in BFO had a significant improvement effect on the magnetic properties, with the remnant magnetization being 0.557 emu g^{-1}, due to the structural phase transition, size effects and the strong ferromagnetic interaction between Fe^{3+}–O–Cr^{3+} ions arising from Cr substitution. Meanwhile, the doping of Dy into BFO effectively reduced the leakage current and enhanced the ferroelectric properties. The simultaneous enhancement of magnetic and ferroelectric properties shows the great potential application of Dy- and Cr-co-doped BFO in future multifunctional devices.

1. Introduction

Multiferroics, which capture great attention for their potential application in multifunctional devices, simultaneously possess ferroic properties, such as ferroelectricity, ferromagnetism and ferroelasticity, coupled with electric, magnetic and structural order parameters.[1–3] So far, several single-phase multiferroics have been developed, such as $YMnO_3$, $BiMnO_3$, $DyMnO_3$ and $BiFeO_3$ (BFO).[4–7] Of those, BFO is known to be the only one with simultaneous ferroelectric ($T_c \sim 1103$ K) and G-type antiferromagnetic ($T_N \sim 643$ K) orderings at room temperature.[8] Its unique multiferroic behaviour renders BFO an ideal candidate for most important multifunctional applications.[9–11] However, bulk BFO is characterized by some inherent problems including a high leakage current, the persistent formation of secondary phases and weak ferromagnetism. The combined action of exchange and spin–orbit interactions produces spin canting away from perfect antiferromagnetic ordering, resulting in a small magnetic moment. However, the direction of the moment would rotate and superimpose a spiral-modulated spin structure with a wavelength of 62 nm, generating a vanishing magnetization in the BFO.[12]

Based on the hypothesis of Spaldin, the ferroelectricity and magnetism of BFO mainly result from lone pair electrons of the Bi^{3+} ions and the magnetism of the Fe^{3+} ions, respectively.[13,14] Hence, several research groups have tried A-site substitution by selected trivalent rare-earth and divalent ions[15–18] or B-site substitution by transition metal ions[19–21] in order to improve the multiferroic properties. It was observed that Dy-doped BFO thin films had significantly enhanced ferroelectric and fatigue properties because of the reduction of oxygen vacancies.[22] In addition, Dy doping was demonstrated to be a very effective method for inducing a weakly ferromagnetic state in the ferroelectric *R3c* phase of BFO in the absence of an external magnetic field.[23] Moreover, it has been reported that Cr^{3+} substitution on the Fe site can enhance the magnetization due to the strong ferromagnetic interaction between Fe^{3+} and Cr^{3+}.[24–26] However, there have been no reports of Dy and Cr co-doping, which may improve both the ferroelectric and magnetic properties in the BFO system.

Herein, we present a carbon microsphere-assisted sol–gel (CSG) method to synthesize Dy- and Cr-co-doped BFO nanoparticles, which exhibit simultaneously enhanced magnetic and ferroelectric properties compared with those of pure BFO. The origins of the improved magnetic and ferroelectric properties are discussed in detail in this work. Meanwhile, we also present

[a] *Key Laboratory for Organic Electronics & Information Displays (KLOEID), Institute of Advanced Materials (IAM), School of Materials Science and Engineering (SMSE), Nanjing University of Posts and Telecommunications (NUPT), Nanjing 210023, P. R. China. E-mail: lxahbmy@126.com, iamwhuang@njupt.edu.cn; Tel: +86-02585866362, +86-02585866533*

[b] *College of Science, Information Physics Research Center, Advanced Energy Technology Center, Nanjing University of Posts and Telecommunications (NUPT), Nanjing 210023, P. R. China*

[c] *Key Laboratory of Flexible Electronics (KLOFE) & Institute of Advanced Materials (IAM), National Synergistic Innovation Center for Advanced Materials (SICAM), Nanjing Tech University (NanjingTech), 30 South Puzhu Road, Nanjing 211816, China*

an analysis of the influence of the introduction of carbon microspheres, which play a role in reducing the grain sizes and in enhancing the magnetic properties. Co-doping Dy and Cr into BFO prepared by a CSG method may thus be an effective way to improve the magnetic and ferroelectric properties.

2. Experimental

2.1. Preparation of carbon microspheres

Carbon microspheres were prepared by a hydrothermal method.[27] Glucose (6.0 g) was dissolved in deionized water (40 mL) with the aid of ultrasonication. The solution was transferred into a Teflon-lined stainless steel autoclave with a 50 mL inner volume, and then loaded into an oven at 180 °C for reaction for 4 h. After the reaction, the obtained products were harvested and washed with deionized water several times *via* centrifugation. Finally, the as-prepared carbon microspheres were dried at 70 °C for two days.

2.2. Preparation of BFO

Polycrystalline samples of pure BFO (BFO-C), $Bi_{0.95}Dy_{0.05}FeO_3$ (Dy5-C) and $Bi_{0.95}Dy_{0.05}Fe_{0.95}Cr_{0.05}O_3$ (Dy5Cr5-C) were synthesized *via* a carbon microsphere-assisted sol–gel method. A schematic illustration of the preparation is shown in Fig. 1. Appropriate proportions of Bi_2O_3, $Fe(NO_3)_3{\cdot}9H_2O$, Dy_2O_3 and $Cr(NO_3)_3{\cdot}9H_2O$ were used as precursor materials, which were dissolved in dilute nitric acid with a chelating agent of tartaric acid. Carbon microspheres (0.08 g) were dispersed in 10 mL distilled water with the aid of ultrasonication for 1 h. For the assistance using the carbon microspheres, the suspension was added drop-by-drop into the above precursor solution of BFO and vigorously stirred for 12 h. Then, the mixed suspension was dried at 70 °C for 24 h and calcined at 600 °C for 2 h. To make a comparison, BFO (BFO), $Bi_{0.95}Dy_{0.05}FeO_3$ (Dy5) and $Bi_{0.95}Dy_{0.05}Fe_{0.95}Cr_{0.05}O_3$ (Dy5Cr5) were also synthesized by a conventional sol–gel (SG) method, as reported in our earlier paper.[28]

2.3. Characterization

The structure and phase purity of the samples were characterized by X-ray diffraction (XRD) using Cu-Kα radiation at room temperature. The morphology and local element occupancy were examined using scanning electron microscopy (SEM, JEOL-6380LV, Japan) and energy-dispersive X-ray spectroscopy (EDS, HORIBA EMAX Energy EX-250). Transmission electron microscopy (TEM) imaging and grain size characterization were performed on a JEOL JEM-2100 microscope, by depositing a drop of sample dispersion onto a 300 mesh Cu grid coated with a carbon layer. Ferroelectric hysteresis loops (*P*–*E*) and leakage current density–electric field (*J*–*E*) curves were measured using a Radiant precision materials analyzer, with each powder sample pressed into a thin piece under a pressure of 20 MPa and having an area of around 0.2 cm^2 and a thickness of around 0.08 cm. Ag electrodes were coated on both sides. Magnetization hysteresis (*M*–*H*) loops were evaluated at room temperature up to a field of 50 kOe using a vibrating sample magnetometer (VSM).

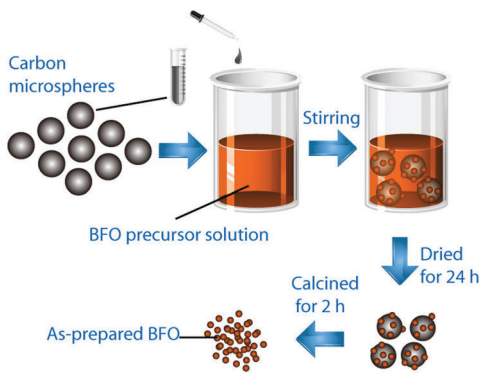

Fig. 1 Schematic illustration of the synthesis of the samples *via* a carbon microsphere-assisted sol–gel method.

3. Results and discussion

The XRD patterns of all the samples are shown in Fig. 2(a). All the diffraction peaks associated with the pure BFO nanoparticles are well matched with a rhombohedral structure (JCPDS file no. 71-2494). Comparing the two methods, there is no difference between the XRD patterns of the samples prepared by different methods. This suggests that the presence of carbon microspheres did not affect the synthesis of BFO and doped BFO. The role of the carbon microspheres additive in decreasing the average grain size of BFO can be explained as follows. There are small amounts of the impurity phase $Bi_2Fe_4O_9$ discernable in the XRD patterns for BFO-C, Dy5Cr5 and Dy5Cr5-C, as marked by "*" in Fig. 2(a). The absence of the diffraction peaks of the oxides of Dy or Cr implies that substitution did not trigger the formation of these impurity phases, thereby meaning that Dy and Cr ions were doped into BFO successfully. An enlarged version of the XRD patterns in the 2θ range of 31°–33° is displayed in Fig. 2(b), which reveals an evolution of the (104) and (110) diffraction peaks. The two peaks are clearly separated in BFO (BFO-C), then show a trend towards coalescence in the Dy5 (Dy5-C) samples. After co-doping with Dy and Cr, the doubly-split peaks merge to form one peak in Dy5Cr5 (Dy5Cr5-C). This phenomenon indicates that substitution induces structural distortion, which can be attributed to the Dy^{3+} ion having a smaller ionic radius than the Bi^{3+} ion and the Cr^{3+} ion having a smaller ionic radius than the Fe^{3+} ion.[29,30] Furthermore, the single Dy doping concentration of 5 mol% only leads to some kind of structural distortion, while co-doping can cause a lattice distortion from the rhombohedral structure to a tetragonal structure. Similar behaviour has also been observed in other reports.[31–33] Elemental analysis was carried out using the EDS analysis. Typical EDS patterns of BFO-C, Dy5-C and Dy5Cr5-C are shown in Fig. 2(c)–(e). The chemical composition of BFO-C agrees with the nominal one, 1 : 1 : 3, approximately. Besides the obvious signals for O, Bi and Fe, the EDS spectra show a weak signal of Dy in Dy5-C and Dy/Cr in Dy5Cr5-C. The measured quantitative values yield atomic percentages of 16.95% Bi and

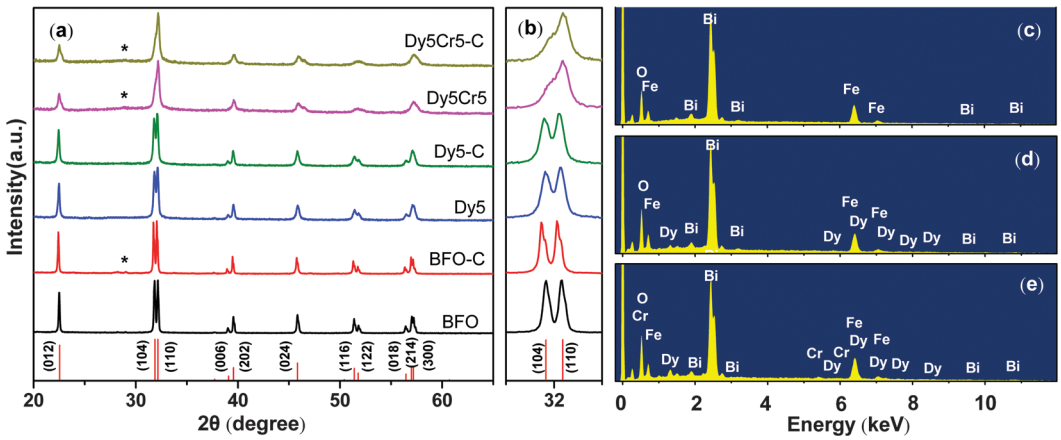

Fig. 2 (a) X-ray diffraction patterns of all the samples at room temperature. (b) Enlarged view of the diffraction peaks (104) and (110). Typical EDS patterns of (c) BFO-C, (d) Dy5-C and (e) Dy5Cr5-C.

1.08% Dy for Dy5-C, and 16.53% Bi, 1.30% Dy, 17.31% Fe and 1.12% Cr for Dy5Cr5-C. According to the above results, it is evident that Dy and Cr ions were effectively incorporated into the host material.

The morphology of the as-synthesized samples was observed by SEM. Fig. 3(a)–(c) show typical surface SEM images of the conventional SG-processed samples. If there were no carbon microspheres, the morphologies were random without any regular particles, and the grain sizes nearly reached the microscale. It was surprising that by the assistance of carbon microspheres, the grain sizes reduced from microscale to nanoscale, as shown in Fig. 3(d)–(f). Additional support was obtained by TEM characterization. Fig. 3(g)–(i) show typical TEM images of BFO-C, Dy5-C and Dy5Cr5-C. Histograms of particle size distribution are shown as the insets of Fig. 3(g)–(i), obtained from TEM images. It could be measured that the average grain sizes of BFO-C, Dy5-C and Dy5Cr5-C were 71.14 nm, 68.26 nm and 69.31 nm, respectively. It was concluded that the carbon microspheres had a significant impact on the formation of uniform BFO particles. It is well known that the agglomeration takes place due to the high surface energy of the nanoparticles. In our experiment, the carbon microspheres became the nucleation sites of the BFO when they were added into the BFO solution, which was illustrated in Fig. 1. BFO nanoparticles were nucleated in the solution, and then they were adsorbed onto the surface of the carbon microspheres, because the surface energy of the carbon microspheres was lower than that of the BFO. After calcination in air to remove the carbon microspheres, the BFO nanoparticles were obtained with effectively reduced grain size and homogeneous microstructures.

Fig. 4(a)–(c) show a comparison of the magnetic hysteresis (M–H) loops for the conventional SG-prepared and CSG-prepared samples at room temperature, with a maximum applied field of 50 kOe. Table 1 summarizes the values of remnant magnetization (M_r), coercive field (H_c) and maximum magnetization (M_s) at 50 kOe, which clearly demonstrate the enhanced magnetic parameters of the samples prepared by the CSG method. The enhancement in ferromagnetism can possibly be attributed to the presence of $Bi_2Fe_4O_9$, because of the weak ferromagnetic properties of $Bi_2Fe_4O_9$ nanoparticles.[34,35] In addition, the enhanced magnetic properties may be attributed to the size effect of the nanoparticles. When the dimensions of BFO particles are decreased to the nanoscale, they start to exhibit a variety of new physical phenomena, such as weak ferromagnetism.[36–38] In accordance with the Nèel theory, the magnetization in an antiferromagnetic material can be described as comprising two spin sublattices with ferromagnetic interactions within one sublattice and antiferromagnetic interactions between sublattices.[39] These materials exhibit measurable magnetization due to incomplete magnetic compensation between these two spin sublattices. This incomplete spin compensation gives rise to a measurable magnetic moment in the case of small antiferromagnetic systems, as the antiferromagnetic ordering gets interrupted at the surface of the particle.[36,37] As the surface to volume ratio becomes larger with decreasing particle size in nanoparticles, the uncompensated spins at the surface contribute substantially towards the enhancement of the particles' overall magnetization.

Substitution is known to be an effective way to enhance the ferromagnetic properties of BFO *via* varying the electronic and crystalline structure. To investigate the effect of substitution on the ferromagnetic properties, the field-dependent magnetization of the three CSG-prepared samples was measured at room temperature and the results are shown in Fig. 4(d). The M–H curves indicate that the ferromagnetic properties of the doped samples are much more enhanced than those of the BFO-C. For pure BFO-C, the magnetization increases linearly with increasing magnetic field, and the maximum magnetization (M_s) at the maximum applied field of 50 kOe corresponds to 0.471 emu g^{-1}, which suggests that the pure BFO is antiferromagnetic.[40] Compared with BFO-C, clear hysteresis loops are observed for the Dy5-C and Dy5Cr5-C samples. There is a slight increase in the maximum magnetization for the sample with the individual substitution of Dy ($M_s \sim 0.765$ emu g^{-1}) compared with that for BFO-C. The highest values of M_s ($\sim$1.542 emu g^{-1}),

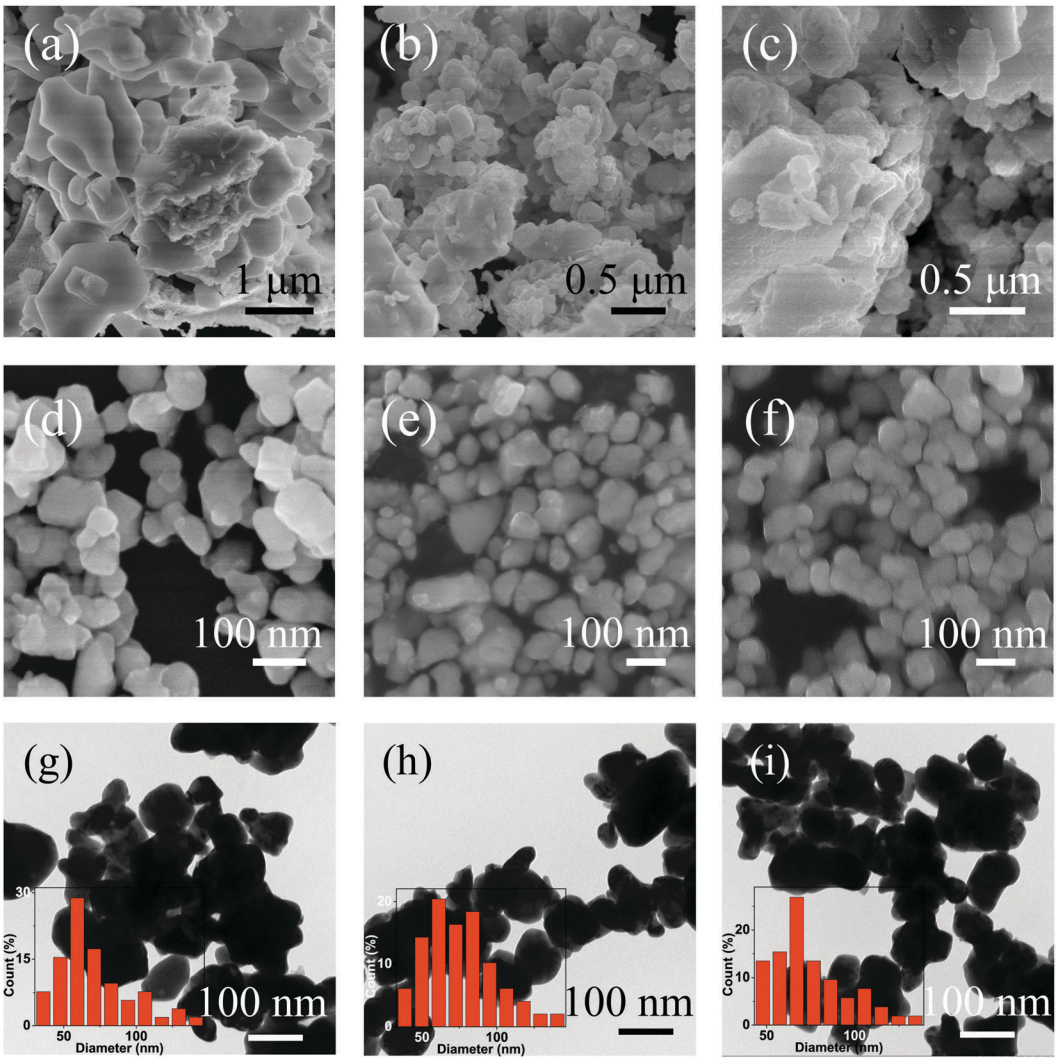

Fig. 3 SEM images for (a) BFO, (b) Dy5, (c) Dy5Cr5, (d) BFO-C, (e) Dy5-C and (f) Dy5Cr5-C. TEM images for (g) BFO-C, (h) Dy5-C and (i) Dy5Cr5-C. The insets in (g–i) show the particle size distributions of BFO-C, Dy5-C and Dy5Cr5-C, respectively.

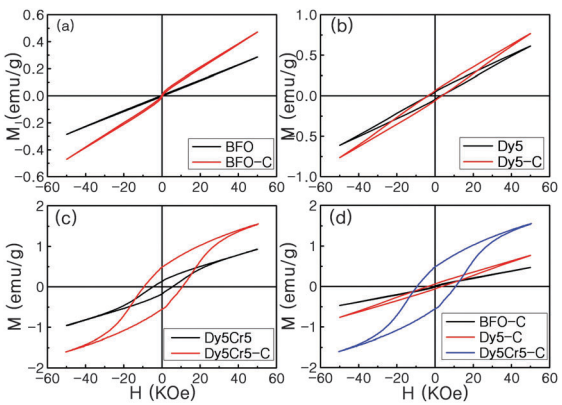

Fig. 4 Room temperature magnetic hysteresis loops for (a) BFO and BFO-C, (b) Dy5 and Dy5-C, (c) Dy5Cr5 and Dy5Cr5-C, and (d) BFO-C, Dy5-C and Dy5Cr5-C.

M_r (~0.557 emu g^{-1}) and H_c (~9.348 kOe) occurred in the double-doped Dy5Cr5-C sample. The origin of weak ferromagnetism in BFO is the spin of the Fe^{3+}, which is responsible for G-type antiferromagnetic ordering modified by a long-range modulation of the cycloidal spiral.[12,41] This cycloidal structure results in the disappearance of the macroscopic magnetization. So the enhanced magnetization in Dy5-C and Dy5Cr5-C could be due to the structural distortion, based on the structural analysis of XRD data. The structural distortion destroyed the spiral spin modulation

Table 1 Magnetic parameters at room temperature

	Maximum magnetization (emu g^{-1})	Remnant magnetization (emu g^{-1})	Coercive field (kOe)
BFO	0.286	0.0033	0.622
BFO-C	0.471	0.0065	0.313
Dy5	0.611	0.0438	3.283
Dy5-C	0.765	0.0580	3.283
Dy5Cr5	0.927	0.174	4.731
Dy5Cr5-C	1.542	0.557	9.348
Dy10-C	1.373	0.243	8.242

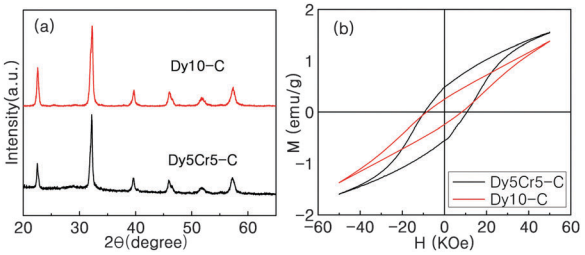

Fig. 5 (a) X-ray diffraction patterns of Dy5Cr5-C and Dy10-C, and (b) magnetic hysteresis loops for Dy5Cr5-C and Dy10-C.

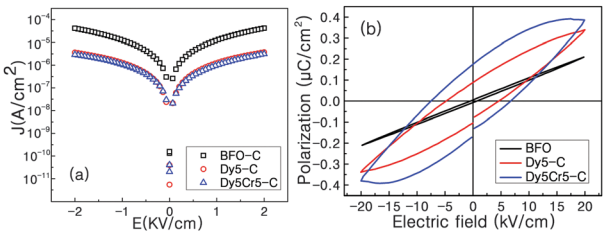

Fig. 6 (a) The leakage current density–electric field behaviour for the BFO-C, Dy5-C and Dy5Cr5-C samples. (b) Polarization hysteresis loops of the BFO-C, Dy5-C and Dy5Cr5-C samples.

in BFO, so that the latent magnetization locked within the cycloid might be released. In the Dy5-C sample, the individual substitution of Dy could only suppress but could not destroy the spin cycloid structure completely, leading to a limited increase of magnetization. However, the Dy and Cr co-doping induced a structural phase transition, wherein the spin cycloid might be destroyed.[42] Therefore, significantly increased magnetization is observed in the Dy5Cr5-C sample.

In order to further analyze and understand the role of Cr doping on the ferromagnetic properties, we prepared $Bi_{0.90}Dy_{0.10}FeO_3$ (Dy10-C) nanoparticles by the same method. The XRD patterns of Dy5Cr5-C and Dy10-C are shown in Fig. 5(a). All the diffraction peaks are almost the same for the two samples. Room-temperature *M–H* loops of Dy5Cr5-C and Dy10-C are shown in Fig. 5(b). The M_s at the maximum applied field of 50 kOe and the M_r for Dy10-C are 1.37 emu g^{-1} and 0.243 emu g^{-1}, respectively. Dy5Cr-C exhibits an enhanced value of M_r of 0.557 emu g^{-1}, which is almost twice that for Dy10-C. In principle, the M_r is due to weak ferromagnetism, attributed to the canting which is caused by the Dzyaloshinsky–Moriya interactions in multiferroic perovskites.[43] Due to the paramagnetic contribution from the Dy ions, the *M–H* loops do not exhibit any saturation for Dy10-C.[29] In contrast to this case, the room-temperature field-dependent magnetization of Dy5Cr-C begins to exhibit some saturation of the magnetization in the highest magnetic fields. From the XRD results, Dy5Cr-C has the similar crystal structure as Dy10-C. So the further increased magnetization of Dy5Cr-C might be due to the substitution of Fe^{3+} by Cr^{3+} rather than structural distortion. As is known to all, BFO presents a weak magnetization because of Fe^{3+}–O–Fe^{3+} antiferromagnetic exchange interactions. When Cr^{3+} ions occupy Fe sites, the ferromagnetic interaction between Fe^{3+}–O–Cr^{3+} ions appears, which plays the key role in the enhancement of the magnetization, especially the larger M_r and H_c. Koval *et al.* reported that the M_r was about 0.21 emu g^{-1} for the $Bi_{0.9}Dy_{0.1}FeO_3$ ceramic synthesized by a solid-state reaction method.[23] Das *et al.* evaluated the magnetic properties of Cr-doped BFO nanotubes, which exhibited weak ferromagnetic behaviour with M_r and H_c values of 0.00054 emu g^{-1} and 0.023 kOe, respectively.[44] Dutta *et al.* synthesized $BiFe_{0.9}Cr_{0.1}O_3$ and $BiFe_{0.9}Mn_{0.1}O_3$ nanorods using a sonochemical technique. The obtained M_r and H_c were around 0.05 emu g^{-1} and 0.35 kOe for $BiFe_{0.9}Cr_{0.1}O_3$, and 0.02 emu g^{-1} and 0.57 kOe for $BiFe_{0.9}Mn_{0.1}O_3$.[36] Apparently, the M_r and H_c of Dy5Cr-C are higher than those of single-doped Dy- or Cr-doped BFO in the earlier works. Furthermore, the values in the present work are well comparable with previous values of BFO doped with Pr, Ho, Eu and Sr elements.[45–47] The promising magnetic properties achieved in the present Dy5Cr-C sample could be associated with the size effect, the structural phase transition and the ferromagnetic interaction between Fe^{3+}–O–Cr^{3+} ions.

Fig. 6(a) shows the leakage current density (J) as a function of the applied electric field (E) for BFO-C, Dy5-C and Dy5Cr5-C, measured at room temperature. It is clear that all the *J–E* curves have good symmetry under positive and negative electric fields. For the pure BFO-C, the leakage current density is 4.19×10^{-5} A cm^{-2} at an applied electric field of 20 kV cm^{-1}. At the same applied electric field, the leakage current density of Dy5-C is 4.17×10^{-6} A cm^{-2}, which is about one order of magnitude lower than that of BFO-C. It can also be obtained from the *J–E* data that Cr doping in Dy5-C does not lead to an obvious change. This clearly reveals that the leakage current density can be effectively reduced by substitution with Dy. As is known to all, the large leakage current density in BFO mainly results from charge defects such as oxygen vacancies. The oxygen vacancies arise due to the volatile nature of Bi at high temperature.[48] Dy substitution, as for other rare earth substituents in the Bi site of BFO, can suppress the formation of oxygen vacancies by controlling the volatility of the Bi atoms and stabilizing the oxygen octahedron.[16] Therefore, the decrease of leakage current density in the two doped samples is mainly due to the reduction in the concentration of oxygen vacancies caused by Dy doping.

To ascertain the ferroelectric behaviour of the BFO-C, Dy5-C and Dy5Cr5-C nanoparticles, the polarization hysteresis (*P–E*) loops were measured under an applied electric field (E) of about 20 kV cm^{-1}, and are shown in Fig. 6(b). It is clearly observed that all the samples show unsaturated *P–E* curves, revealing high leakage currents. As is known, the high leakage current in BFO mainly originates from charge defects such as bismuth vacancies or oxygen vacancies. The oxygen vacancies arise due to Bi deficiency, given its highly volatile nature, and the valence fluctuations of Fe.[48] For the pure BFO-C, a linear *P–E* loop with weak remnant polarization 2Pr (0.0146 μC cm^{-2}) was observed. Compared with BFO-C, a significant improvement of the ferroelectric properties can be observed in the substitution products. The 2Pr and the coercive electric field (E_c) of the Dy-doped BFO were 0.210 μC cm^{-2} and 4.807 kV cm^{-1}, respectively.

Better ferroelectric properties were exhibited in Dy5Cr5-C; both 2Pr and E_c increased, to 0.370 μC cm^{-2} and 7.511 kV cm^{-1}, respectively. As confirmed by the *J–E* curves, Dy substitution can suppress the oxygen vacancies, and therefore decrease the leakage current density and enhance the ferroelectric behaviour of BFO. Furthermore, the origin of ferroelectricity in BFO is generally due to the Bi^{3+} ($6s^2$) lone pair electrons.[49] The stereochemical activity of the lone pair will be enhanced by the structural transition as a result of Dy- and Cr-co-doping in BFO indicated by the XRD patterns.[50] Therefore, the structural transition might be another reason for the better ferroelectric properties of the Dy5Cr5-C nanoparticles.

4. Conclusion

In summary, an innovative approach for preparing Dy- and Cr-co-doped BFO nanoparticles by a carbon microsphere-assisted sol–gel (CSG) method is presented in this paper. The XRD results show the formation of an impurity phase by the addition of carbon microspheres, and a phase transition from a rhombohedral to a tetragonal structure arising from co-doping Dy and Cr into BFO. Compared with the conventional SG-prepared samples, the grain sizes of the CSG-prepared samples reached the nanoscale, with average sizes of 71.14 nm for BFO-C and 69.31 nm for Dy5Cr5-C. The Dy5Cr5-C nanoparticles exhibited greatly enhanced magnetic and ferroelectric properties. All these results suggest that the CSG method and the co-doping of Dy and Cr in BFO are an effective way to improve the magnetic and ferroelectric properties, which is essential for practical applications.

Acknowledgements

We acknowledge the financial support from the Ministry of Education of China (No. IRT1148), the National Synergistic Innovation Center for Advanced Materials (SICAM), the Natural Science Foundation of Jiangsu Province, China (BM2012010), the Project Funded by the Priority Academic Program Development of Jiangsu Higher Education Institutions (PAPD, YX03001), Science and Technology Innovation on Training Program (STITP, SZDG2014018) and the National Natural Science Foundation of China (51172110, 51372119, 61377019, 61136003, 51173081), College Postgraduate Research and Innovation Project of Jiangsu Province (KYLX_0794, KYLX15_0848), the Natural Science Foundation of Scientific and Technological Department of Jiangsu Province (KZ0070715050), the Seed Project Funded by Introducing Talent of NJUPT (XK0070915022), and the Natural Science Foundation of NJUPT (NY214129, NY214130, NY214181).

Notes and references

1 W. Eerenstein, N. D. Mathur and J. F. Scott, *Nature*, 2006, **442**, 759–765.
2 S. W. Cheong and M. Mostovoy, *Nat. Mater.*, 2007, **6**, 13–20.
3 J. Ma, J. Hu, Z. Li and C. W. Nan, *Adv. Mater.*, 2011, **23**, 1062–1087.
4 T. Ahmad, I. H. Lone and M. Ubaidullah, *RSC Adv.*, 2015, **5**, 58065–58071.
5 B. Sun and C. M. Li, *Phys. Chem. Chem. Phys.*, 2015, **17**, 6718–6721.
6 J. Magesh, P. Murugavel, R. V. K. Mangalam, K. Singh, C. Simon and W. Prellier, *J. Appl. Phys.*, 2015, **118**, 074102.
7 B. Sun, L. J. Wei, H. W. Li and P. Chen, *J. Mater. Chem. C*, 2014, **2**, 7547–7551.
8 J. Wang, J. B. Neaton, H. Zheng, V. Nagarajan, S. B. Ogale, B. Liu, D. Viehland, V. Vaithyanathan, D. G. Schlom, U. V. Waghmare, N. A. Spaldin, K. M. Rabe, M. Wuttig and R. Ramesh, *Science*, 2003, **299**, 1719–1722.
9 B. Sun, Y. H. Liu, W. X. Zhao and P. Chen, *RSC Adv.*, 2015, **5**, 13513–13518.
10 R. Guo, L. You, Y. Zhou, Z. S. Lim, X. Zou, L. Chen, R. Ramesh and J. Wang, *Nat. Commun.*, 2013, **4**, 1990.
11 X. F. Wang, W. W. Mao, J. Zhang, Y. M. Han, C. Y. Quan, Q. X. Zhang, T. Yang, J. P. Yang, X. A. Li and W. Huang, *J. Colloid Interface Sci.*, 2015, **448**, 17–23.
12 I. Sosnowska, T. P. Neumaier and E. Steichele, *J. Phys. C: Solid State Phys.*, 1982, **15**, 4835–4846.
13 K. F. Wang, J. M. Liu and Z. F. Ren, *Adv. Phys.*, 2009, **58**, 321–448.
14 A. Filippetti and N. A. Hill, *Phys. Rev. B: Condens. Matter Mater. Phys.*, 2002, **65**, 195120.
15 I. Levin, M. G. Tucker, H. Wu, V. Provenzano, C. L. Dennis, S. Karimi, T. Comyn, T. Stevenson, R. I. Smith and I. M. Reaney, *Chem. Mater.*, 2011, **23**, 2166–2175.
16 N. Jeon, D. Rout, I. W. Kim and S.-J. L. Kang, *Appl. Phys. Lett.*, 2011, **98**, 072901.
17 F. Gao, Y. Yuan, K. F. Wang, X. Y. Chen, F. Chen, J. M. Liu and Z. F. Ren, *Appl. Phys. Lett.*, 2006, **89**, 102506.
18 J. Schiemer, R. L. Withers, M. A. Carpenter, Y. Liu, J. L. Wang, L. Noren, Q. Li and W. Hutchison, *J. Phys.: Condens. Matter*, 2012, **24**, 125901.
19 Q. Y. Xu, H. F. Zai, D. Wu, T. Qiu and M. X. Xu, *Appl. Phys. Lett.*, 2009, **95**, 112510.
20 A. A. Belik, A. M. Abakumov, A. A. Tsirlin, J. Hadermann, J. Kim, G. Van Tendeloo and E. Takayama-Muromachi, *Chem. Mater.*, 2011, **23**, 4505–4514.
21 X. W. Tang, J. M. Dai, X. B. Zhu and Y. P. Sun, *J. Alloys Compd.*, 2013, **552**, 186–189.
22 W. Gao, W. Y. Xing, Q. Yun, J. Y. Chen, C. H. Nie and S. F. Zhao, *J. Mater. Sci.: Mater. Electron.*, 2014, **26**, 2127–2133.
23 V. Koval, I. Skorvanek, M. Reece, L. Mitoseriu and H. Yan, *J. Eur. Ceram. Soc.*, 2014, **34**, 641–651.
24 D. H. Kim, H. N. Lee, M. D. Biegalski and H. M. Christen, *Appl. Phys. Lett.*, 2007, **91**, 042906.
25 B. C. Luo, C. L. Chen, Z. Xu and Q. Xie, *Phys. Lett. A*, 2010, **374**, 4265–4268.
26 S. Godara, N. Sinha and B. Kumar, *Mater. Lett.*, 2014, **136**, 441–444.
27 X. M. Sun and Y. D. Li, *Angew. Chem., Int. Ed.*, 2004, **43**, 597–601.
28 W. W. Mao, X. W. Wang, Y. M. Han, X. A. Li, Y. T. Li, Y. F. Wang, Y. W. Ma, X. M. Feng, T. Yang, J. P. Yang and W. Huang, *J. Alloys Compd.*, 2014, **584**, 520–523.

29 V. A. Khomchenko, D. V. Karpinsky, A. L. Kholkin, N. A. Sobolev, G. N. Kakazei, J. P. Araujo, I. O. Troyanchuk, B. F. O. Costa and J. A. Paixão, *J. Appl. Phys.*, 2010, **108**, 074109.
30 G. H. Dong, G. Q. Tan, W. L. Liu, A. Xia and H. J. Ren, *Ceram. Int.*, 2014, **40**, 1919–1925.
31 P. Godara, A. Agarwal, N. Ahlawat, S. Sanghi and R. Dahiya, *J. Alloys Compd.*, 2014, **594**, 175–181.
32 Y. F. Cui, Y. G. Zhao, L. B. Luo, J. J. Yang, H. Chang, M. H. Zhu, D. Xie and T. L. Ren, *Appl. Phys. Lett.*, 2010, **97**, 222904.
33 V. F. Freitas, L. F. Cótica, I. A. Santos, D. Garcia and J. A. Eiras, *J. Eur. Ceram. Soc.*, 2011, **31**, 2965–2973.
34 T. Maity, S. Goswami, D. Bhattacharya and S. Roy, *Phys. Rev. Lett.*, 2013, **110**, 107201.
35 D. P. Dutta, C. Sudakar, P. S. V. Mocherla, B. P. Mandal, O. D. Jayakumar and A. K. Tyagi, *Mater. Chem. Phys.*, 2012, **135**, 998–1004.
36 D. P. Dutta, O. Jayakumar, A. Tyagi, K. Girija, C. Pillai and G. Sharma, *Nanoscale*, 2010, **2**, 1149–1154.
37 M. M. Shirolkar, R. Das, T. Maity, P. Poddar and S. K. Kulkarni, *J. Phys. Chem. C*, 2012, **116**, 19503–19511.
38 T. J. Park, G. C. Papaefthymiou, A. J. Viescas, A. R. Moodenbaugh and S. S. Wong, *Nano Lett.*, 2007, **7**, 766–772.
39 L. Néel, *Acad. Sci., Paris, C. R.*, 1961, **252**, 4075.
40 D. Lebeugle, D. Colson, A. Forget, M. Viret, A. Bataille and A. Gukasov, *Phys. Rev. Lett.*, 2008, **100**, 227602.
41 G. Catalan and J. F. Scott, *Adv. Mater.*, 2009, **21**, 2463–2485.
42 W. W. Mao, X. A. Li, Y. T. Li, X. W. Wang, Y. F. Wang, Y. W. Ma, X. M. Feng, T. Yang and J. P. Yang, *Mater. Lett.*, 2013, **97**, 56–58.
43 C. D. Hu, *Phys. Rev. B*, 2008, **77**, 174418.
44 R. Das, G. Gopal Khan and K. Mandal, *J. Appl. Phys.*, 2012, **111**, 104115.
45 N. H. Hong, N. Thu Huong, T. Y. Kim, S. Goumri-Said and M. B. Kanoun, *J. Phys. Chem. C*, 2015, **119**, 14351–14357.
46 D. Kothari, V. Raghavendra Reddy, A. Gupta, C. Meneghini and G. Aquilanti, *J. Phys.: Condens. Matter*, 2010, **22**, 356001.
47 D. P. Dutta, B. P. Mandal, R. Naik, G. Lawes and A. K. Tyagi, *J. Phys. Chem. C*, 2013, **117**, 2382–2389.
48 X. Qi, J. Dho, R. Tomov, M. G. Blamire and J. L. MacManus-Driscoll, *Appl. Phys. Lett.*, 2005, **86**, 2903.
49 S. W. Cheong and M. Mostovoy, *Nat. Mater.*, 2007, **6**, 13–20.
50 H. M. Christen, J. H. Nam, H. S. Kim, A. J. Hatt and N. A. Spaldin, *Phys. Rev. B: Condens. Matter Mater. Phys.*, 2011, **83**, 144107.